Synthesis and characterization of RNA containing a rigid and non-perturbing cytidine-derived spin label

Claudia Höbartner,[†]* Giuseppe Sicoli,[‡] Falk Wachowius,[†] Dnyaneshwar B. Gophane,[§] and Snorri Th. Sigurdsson[§]*

[†] Research Group Nucleic Acid Chemistry, Max Planck Institute for Biophysical Chemistry, Am Fassberg 11, 37077 Göttingen, Germany
[‡] Research Group Electron Paramagnetic Resonance, Max Planck Institute for Biophysical Chemistry, Am Fassberg 11, 37077 Göttingen, Germany
[§] Science Institute, University of Iceland, Dunhaga 3, 107 Reykjavik, Iceland

Supporting Information

Table of Contents

List of abbreviations

CD	circular dichroism
CE	2-cyanoethyl
CW	continuous-wave
DMAP	4-dimethylaminopyridine
DME	1,2-dimethoxyethane
DMSO	dimethylsulfoxide
DMTCl	4,4′-dimethoxytrityl chloride
EPR	electron paramagnetic resonance
ESI-MS	electrospray ionization mass spectrometry
HPLC	high performance liquid chromatography
HR-ESI-MS	high resolution electrospray ionization mass spectrometry
NBS	N-Bromosuccinimide
NMR	nuclear magnetic resonance
TBAF	tetrabutylammonium fluoride
tBuOOH	*tert*-butylhydroperoxide
TOM	(triisopropylsilyloxy)methyl
UV	ultraviolet–visible

Table S1. ESI-MS characterization of RNA oligonucleotides.

Name	5'-Sequence-3'	spin label	mol.wt. expected	mol.wt. found
8	GACCUCG**C**AUCGUG	-	4421.7	4421.1
8Cm	GACCUCG**Cm**AUCGUG	-	4435.7	4435.4
8Çm	GACCUCG**Çm**AUCGUG	Çm[8]	4637.9	4638.6
9	CACGAUGCGAGGUC	-	4484.8	4484.8
10	GACGUCGGAAGACGUCAGUA	-	6469.0	6469.5
10aCm	GACGU**Cm**GGAAGACGUCAGUA	-	6483.0	6483.7
10aÇm	GACGU**Çm**GGAAGACGUCAGUA	Çm[6]	6685.0	6685.8
10bCm	GACGU**Cm**GGAAGACGU**Cm**AGUA	-	6497.0	6498.3
10bÇm	GACGU**Çm**GGAAGACGU**Çm**AGUA	Çm[6,16]	6901.5	6902.5
11	UACUGACGUCUUCCGACGUC	-	6279.8	6280.6
11aCm	UACUGA**Cm**GUCUUCCGACGUC	-	6295.8	6295.1
11aÇm	UACUGA**Çm**GUCUUCCGACGUC	Çm[7']	6496.0	6497.1
12	GAUGCGCAAGCAUCUACU	-	5715.5	5715.4
13	AGUAGAUCCGAAAGGAUC	-	5802.6	5802.7
14	GACGUC	-	1874.2	1873.6
15	GACGUCGGA	-	2893.8	2893.4

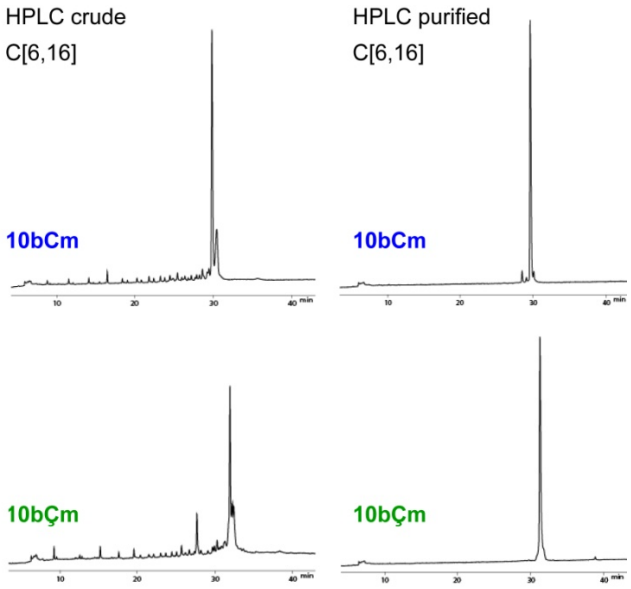

Figure S1. Anion exchange HPLC traces of crude and purified C[6,16]-modified RNAs **10bCm** and **10bÇm.**

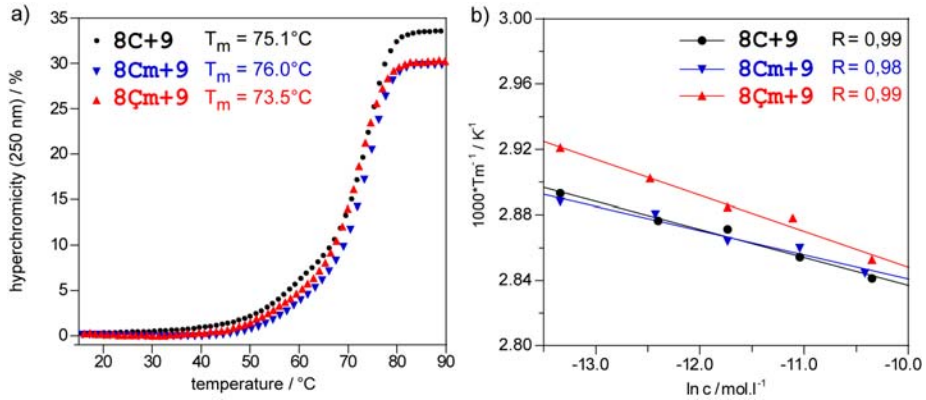

Figure S2. a) UV-melting curves of duplexes **8**+**9** monitored at 250 nm, 8 µM strand concentration, 150 mM NaCl, 10 mM sodium phosphate buffer, pH 7.0. b) Van't Hoff plot (ln(c) versus $1/T_m$) for 14-bp duplexes **8**+**9**. Linear fit parameters and ΔH and ΔS determined from slope and intercept of the linear fit are in Table S2.

Table S2. Thermodynamic data for 14-bp duplexes **8**+**9** (van't Hoff plot ln(c) versus $1/T_m$ in Figure S2)

Modification	slope $(R/\Delta H)$ (10^{-3})	intercept $\frac{\Delta S - R\ln 4}{\Delta H}$ (10^{-3})	R^2	ΔH [kcal/mol]	ΔS [cal/mol.K]	ΔG^{298} [kcal/mol]	$\lvert\Delta\Delta G^{298}\rvert$[a] [kcal/mol]
C(unmodified)	-0.0171	2.666	0.991	-114	-302	-24.4	
Cm[8]	-0.0147	2.664	0.981	-141	-378	-28.2	3.8
Çm[8]	-0.0219	2.629	0.992	-90.5	-235	-20.4	4.0

[a] difference to unmodified RNA

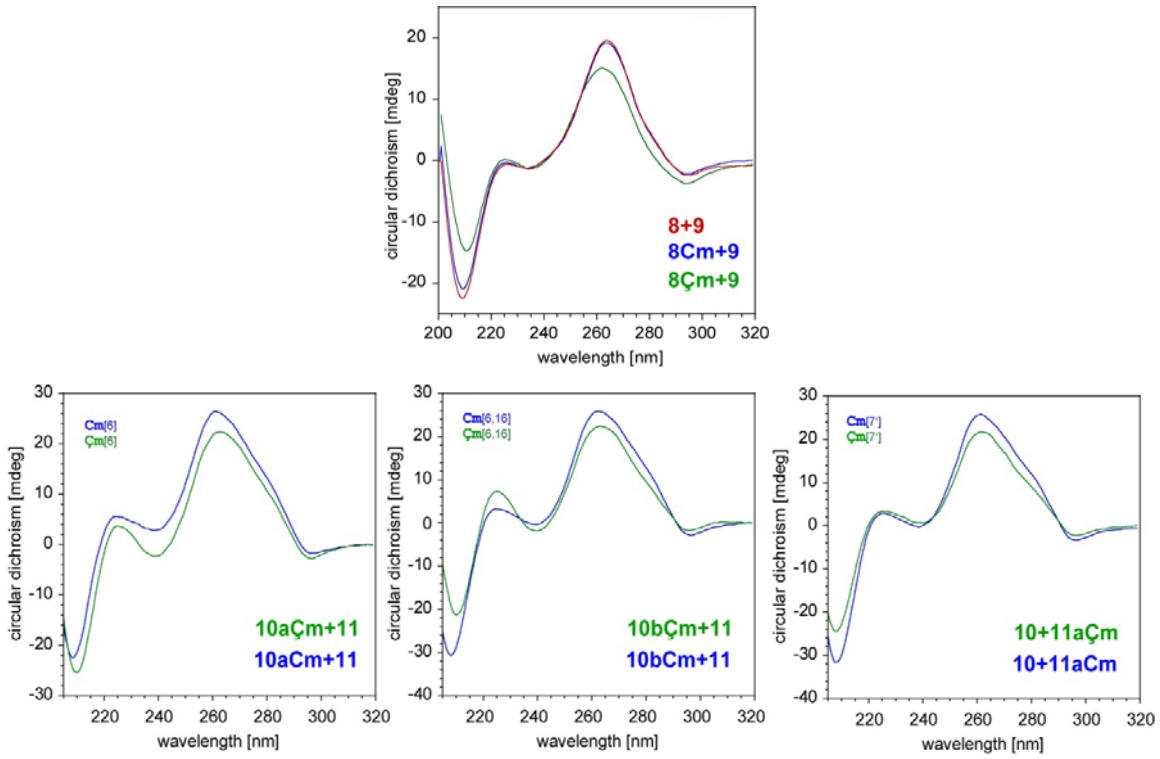

Figure S3. top: CD spectra of model duplex **8**+**9**, 10 µM duplex in 10 mM potassium phosphate buffer, pH 7.0, 150 mM NaCl, at 25°C. bottom row: CD spectra of **Cm** and **Çm** modified 20bp-duplex RNAs, 40 µM duplex in 10 mM potassium phosphate buffer, pH 7.0, 150 mM NaCl, at 25°C.

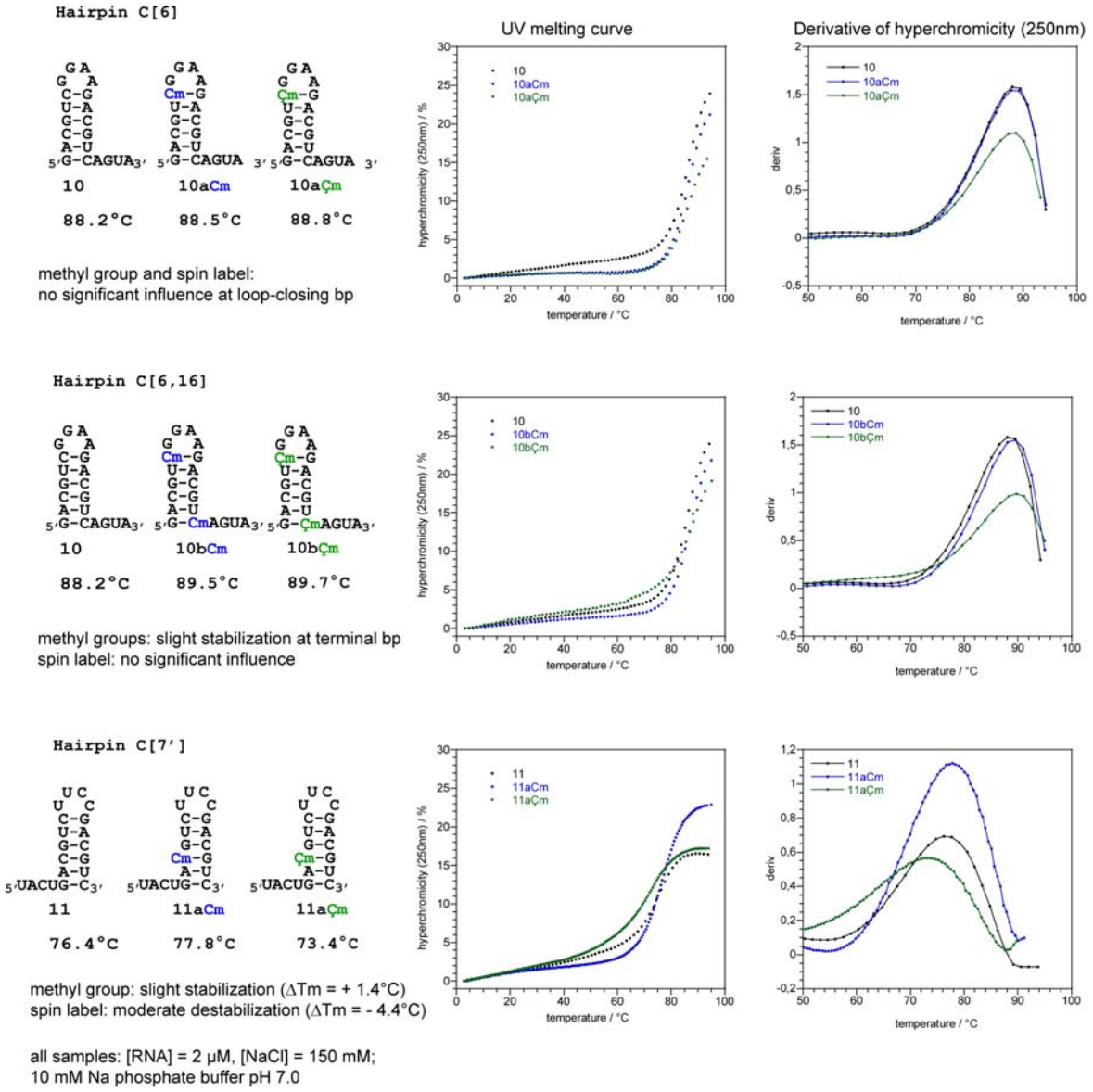

Figure S4. UV melting curve analysis of hairpin RNAs.

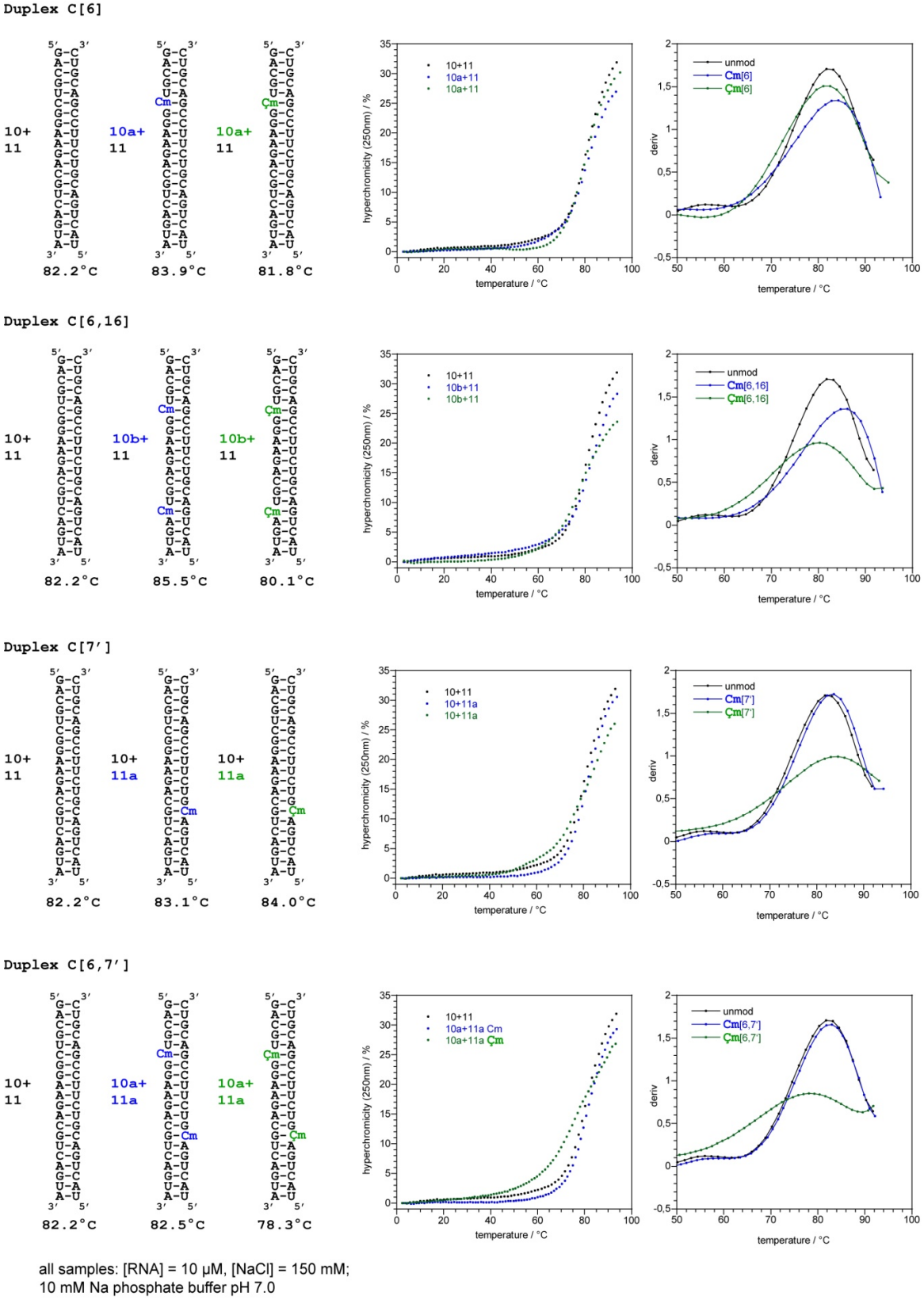

Figure S5. UV melting curve analysis of 20bp-duplex RNAs.

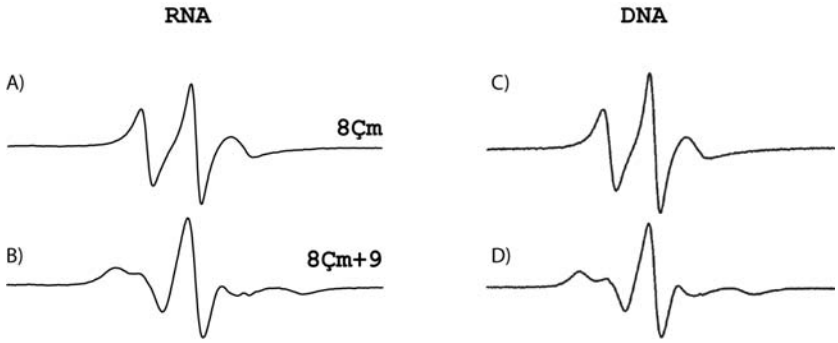

Figure S6. CW-EPR spectra of A) single-strand **8Çm** and B) duplex **8Çm+9**; 25 µM **Çm**-labeled RNA, 150 mM NaCl, 10 mM sodium phosphate buffer, pH 7.0, 23°C. For comparison, CW-EPR spectra of analogous **Ç**-labeled DNA samples are shown. D) single-strand GACCTCG**Ç**ATCGTG, D) duplex (GACCTCG**Ç**ATCGTG).(CACGATGCGAGGTC). Spectra in A) and B) are same as in Figure 2b; spectra in C) and D) are reproduced from Barhate et al., Angew. Chem. Int. Ed. 2007, 46, 2655.

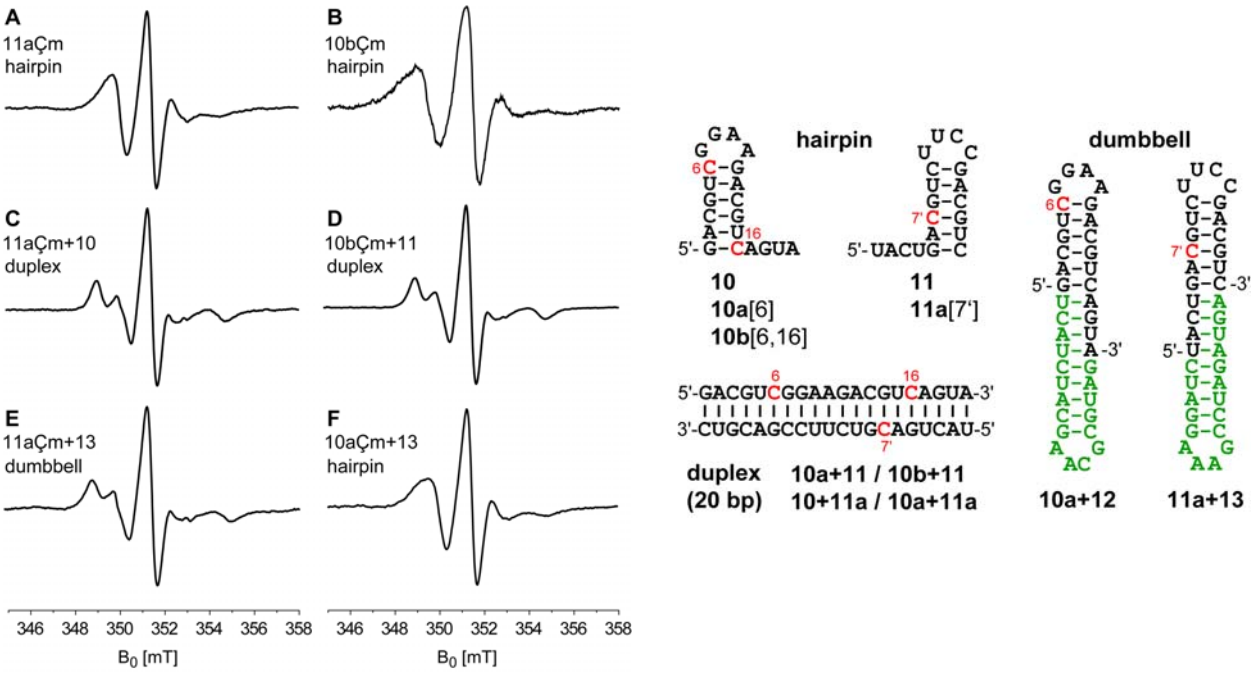

Figure S7. Additional CW-EPR spectra of **Çm**-labeled hairpin, duplex and dumbell RNAs. Spectra were recorded at X-band (9 GHz) over 160 G at 23°C with RNA conc. of 10-25 µM in 10 mM sodium phosphate buffer, pH 7.0 containing 150 mM NaCl. For convenience, Figure 3 of the manuscript is reproduced to the right, showing RNA sequences and secondary structure contexts.

Table S3. Hyperfine values and central line widths of CW-EPR spectra depicted in Figure 4, S7, S10.

Number	label	structure [label position]	base-pairs	central line width ΔH_0[mT]	hyperfine value $2A_{zz}$ [mT]
10a	**C^T**	hairpin [6]	6	0.29	3.93
10a+11	**C^T**	duplex [6]	20	0.37	4.86
10a+12	**C^T**	dumbbell [6]	15	0.35	3.93
10a	**Çm**	hairpin [6]	6	0.50	5.48
10a+11	**Çm**	duplex [6]	20	0.50	6.26
10a+12	**Çm**	dumbbell [6]	15	0.49	6.17
11a	**Çm**	hairpin [7']	6	0.46	5.16
10+11a	**Çm**	duplex [7']	20	0.48	6.22
11a+13	**Çm**	dumbbell [7']	15	0.47	6.18
11a+14	**Çm**	tethered duplex [7']	6/12	0.45	4.98
11a+15	**Çm**	gapped duplex [7']	8/17	0.46	6.13
10a+11a	**Çm**	duplex [6,7']	20	0.46	6.24

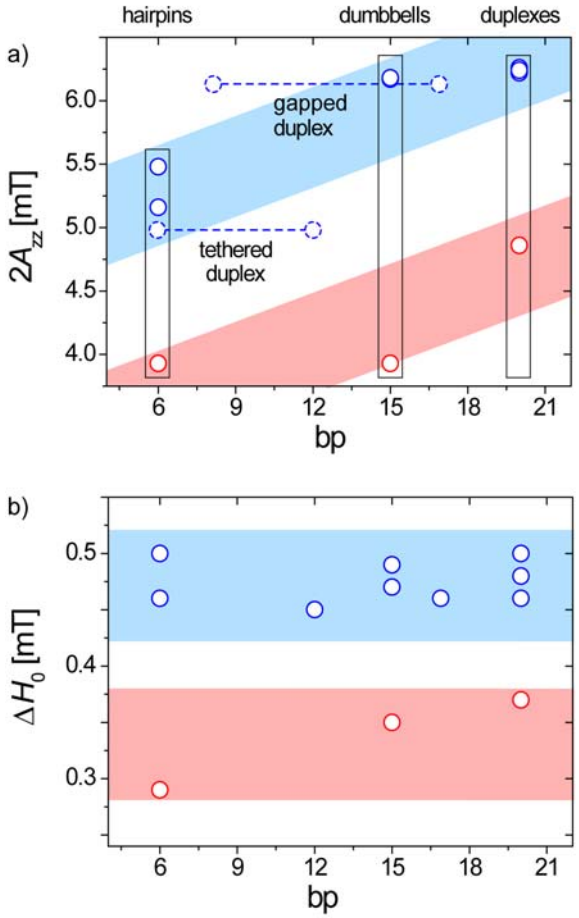

Figure S8. Graphic depiction of a) hyperfine values ($2A_{zz}$) and b) width of the central line (ΔH_0) as a function of the number of base-pairs in **Çm** (blue)- and **C^T** (red)-labeled RNA structures. Tri-molecular structures are represented using outlined symbols with connecting lines between the number of base-pairs in the spin-labeled stem (i.e., 6 bp in the tethered duplex **11**+**14**, and 8 bp in the gapped duplex **11**+**15**) and the total number of base-pairs in each construct. This representation helps to visualize that the mobility of the tethered duplex is more closely related to the hairpin structure (which also contains a 6-bp stem), while the 2Azz value for the gapped duplex fits better into the region for a duplex containing 17 base-pairs. The numerical data are given in Table S3.

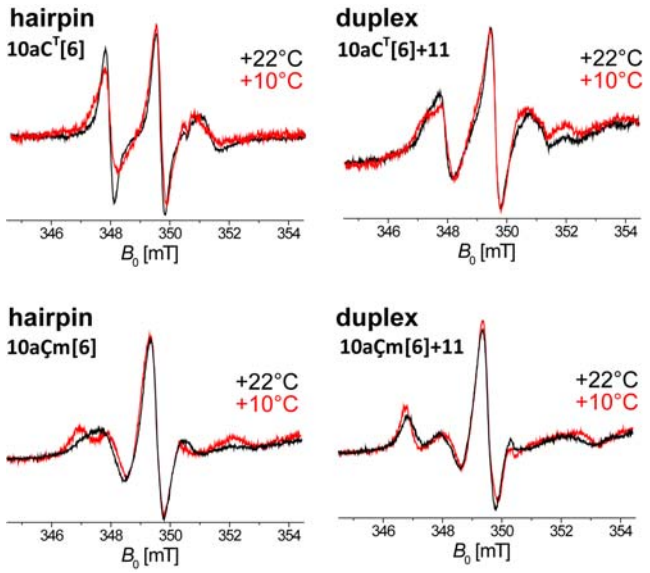

Figure S9. CW-EPR spectra of **C^T**- (top) and **Çm**-(bottom) labeled hairpin RNAs **10a** (left) and duplex **10a+11** (right). Spectra are compared at 22°C (black line) and 10°C (red line). CW EPR measurements at variable temperatures were carried out at 9 GHz using a Varian E-12 ESR spectrometer with nitrogen gas flow temperature regulation. Samples were contained in 1-mm i.d. glass capillaries which were immersed in silicone oil to improve thermal stability. The sample temperature was measured with a thermocouple placed inside the quartz tube just above the top of the ESR cavity.

The spectrum of the **C^T**-labeled hairpin RNA **10a** was not significantly affected by lowering the temperature, which suggests a low energy barrier for spin-label rotation. Also in the duplex **10aC^T+11**, only a minor change in line width was observed. In contrast, spectral broadening and significant splitting of the low field component was observed for the **Çm**-labeled hairpin structure **10aÇm**. This result also supports the finding that the internal local motion of the **C^T** label is much higher than the mobility of the **Çm** label. At a temperature difference of only 12°C, this pronounced effect is not due to changes in sample viscosity, and therefore likely reflects decreased local dynamics of the loop-closing base-pair in the hairpin, which can only be monitored by the new label **Çm**.

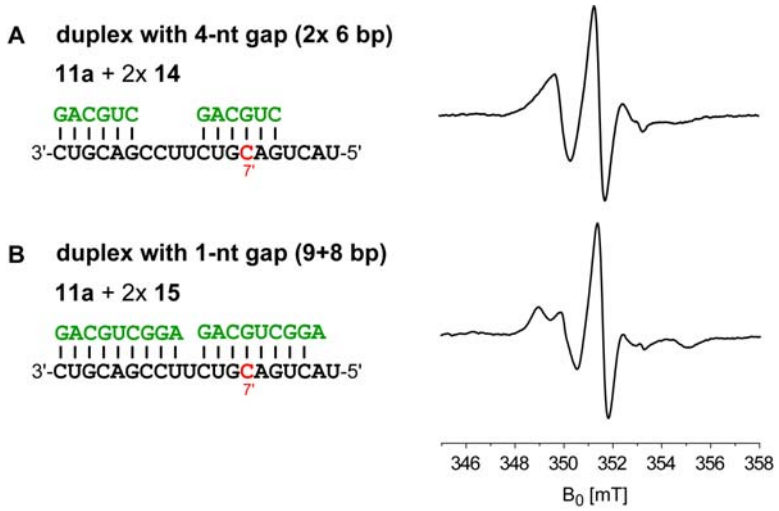

Figure S10. Tri-molecular RNA structures investigated. Secondary structures and CW-EPR spectra of gapped duplexes. Spectra were recorded at X-band (9 GHz) over 160 G at 23°C with RNA conc. of 25 µM in 10 mM sodium phosphate buffer, pH 7.0 containing 150 mM NaCl.

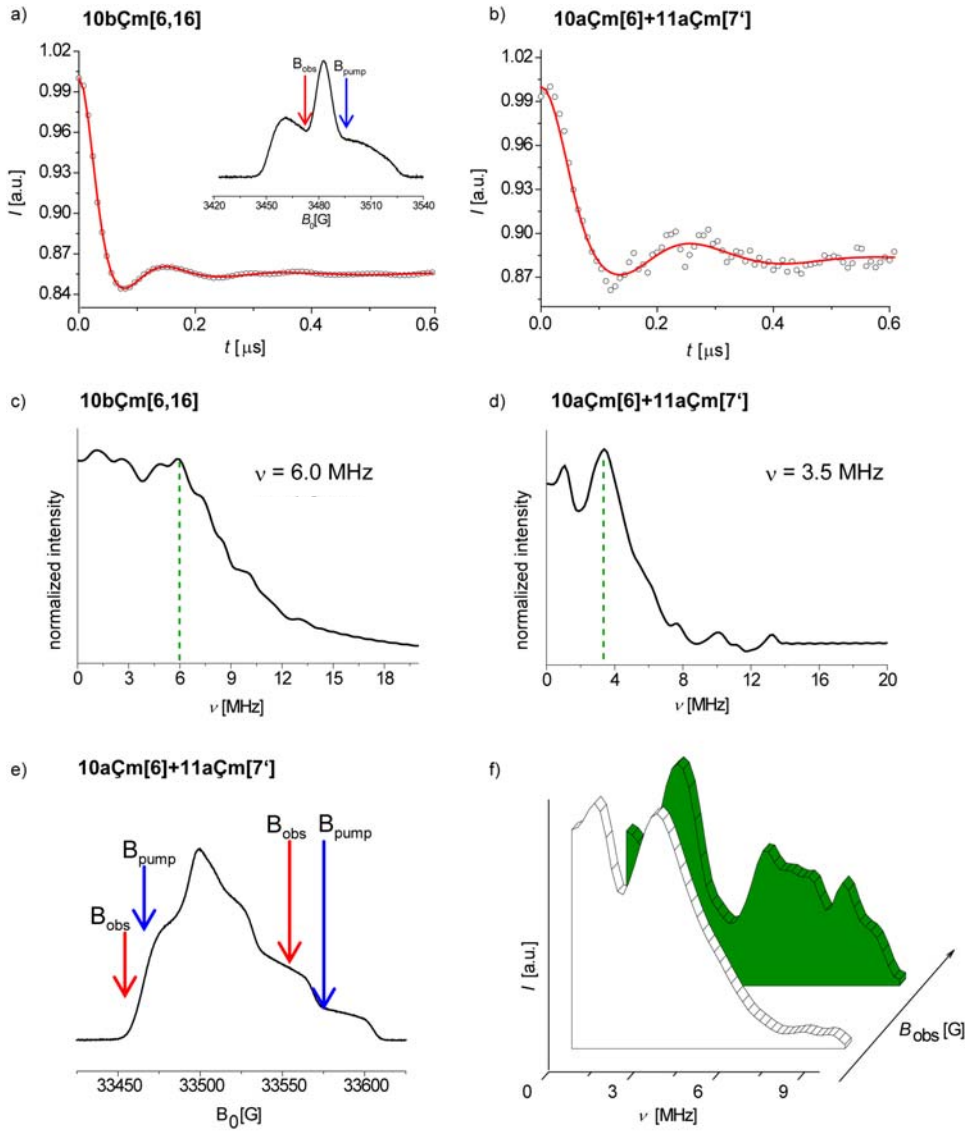

Figure S11. Pulsed electron double resonance (PELDOR) experiments for double-labeled RNA. Dipolar evolution functions at 9 GHz of a) double-**Çm**-labeled hairpin **10bÇm** and b) double-labeled duplex **10aÇm+11aÇm**. The inset in a) shows the 9 GHz ESE spectrum, and indicates the difference between pump and observe pulses (65 MHz). All experiments were performed using the four-pulse PELDOR sequence $\pi/2(\nu_1)\_\tau_1\_\pi(\nu_1)\_\tau_0\_\pi(\nu_2)\_(\tau_1+\tau_2\_\tau_0)\_\pi(\nu_1)\_\tau_2\_$ echo. Parameters (9 GHz): T = 50 K, $\pi/2$ = 16 ns, π = 32 ns, π_{ELDOR} = 36 ns, SPP = 20, SRT = 5 ms, 100 scans; [c] = 50 µM. c) and d) Fourier-transformed dipolar spectra at X-band (Pake patterns) of experiments shown in a) and b), respectively. The green lines indicate the frequencies $\nu_\perp$, corresponding to inter-spin distances of 2.0 nm and 2.5 nm, respectively. e) 94 GHz ESE spectrum of double-labeled duplex **10aÇm+11aÇm**. The arrows indicate two sets of pump and observe pulses, used for detection of PELDOR data shown in f). The parameters for the 94 GHz PELDOR experiment were: T = 40 K, $\pi/2$ = 24 ns, π_{ELDOR} = 56 ns, SRT = 15 ms, 30 scans/trace; [c] = 60 µM. The Pake patterns in c), d), and f) display clear orientation selection, which is currently being analyzed in detail using orientation selection PELDOR experiments at high-field with fixed and variable frequency separation (G. Sicoli et al, manuscript in preparation).

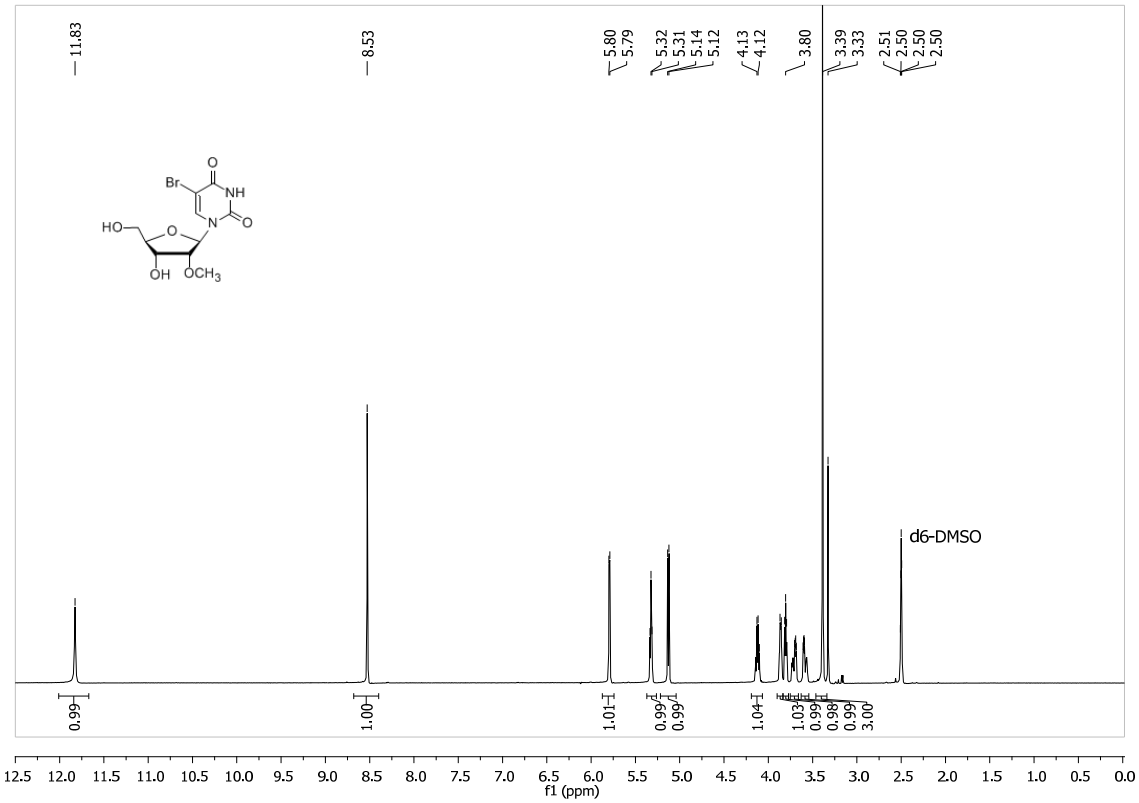

Figure S12. ^{1}H NMR spectrum of **2**

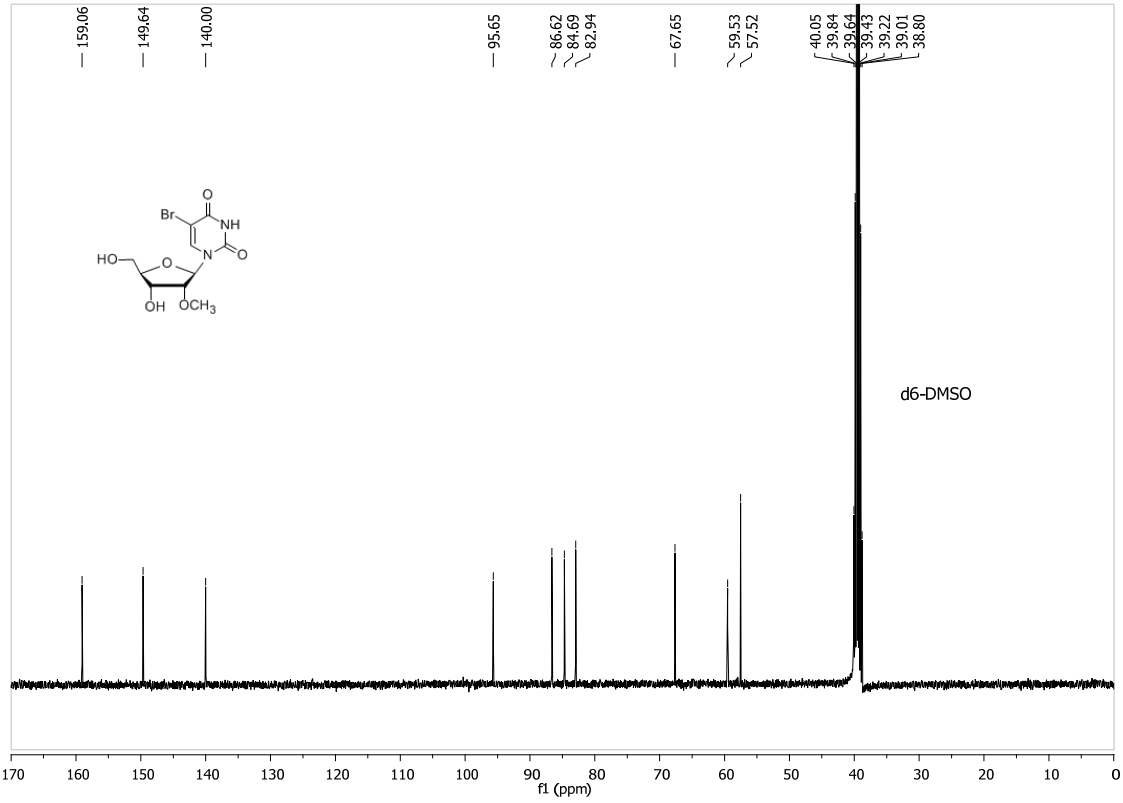

Figure S13. ^{13}C NMR spectrum of **2**

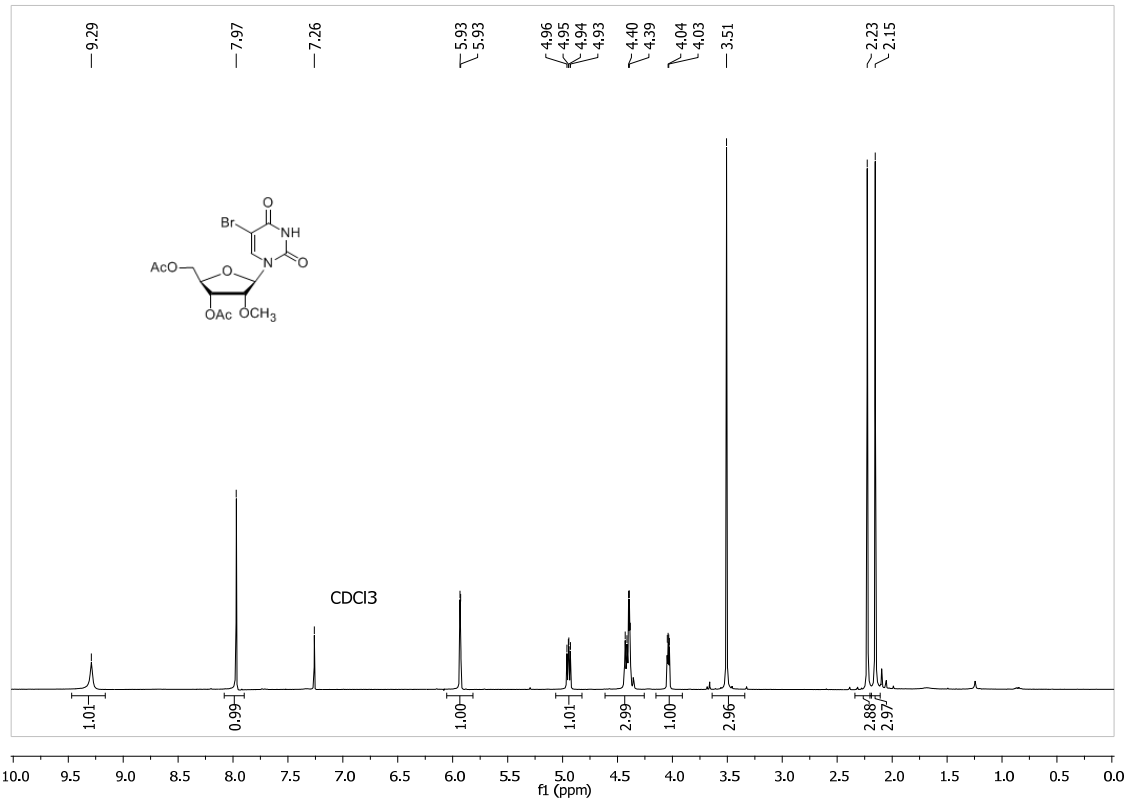

Figure S14. ^{1}H NMR spectrum of **3**

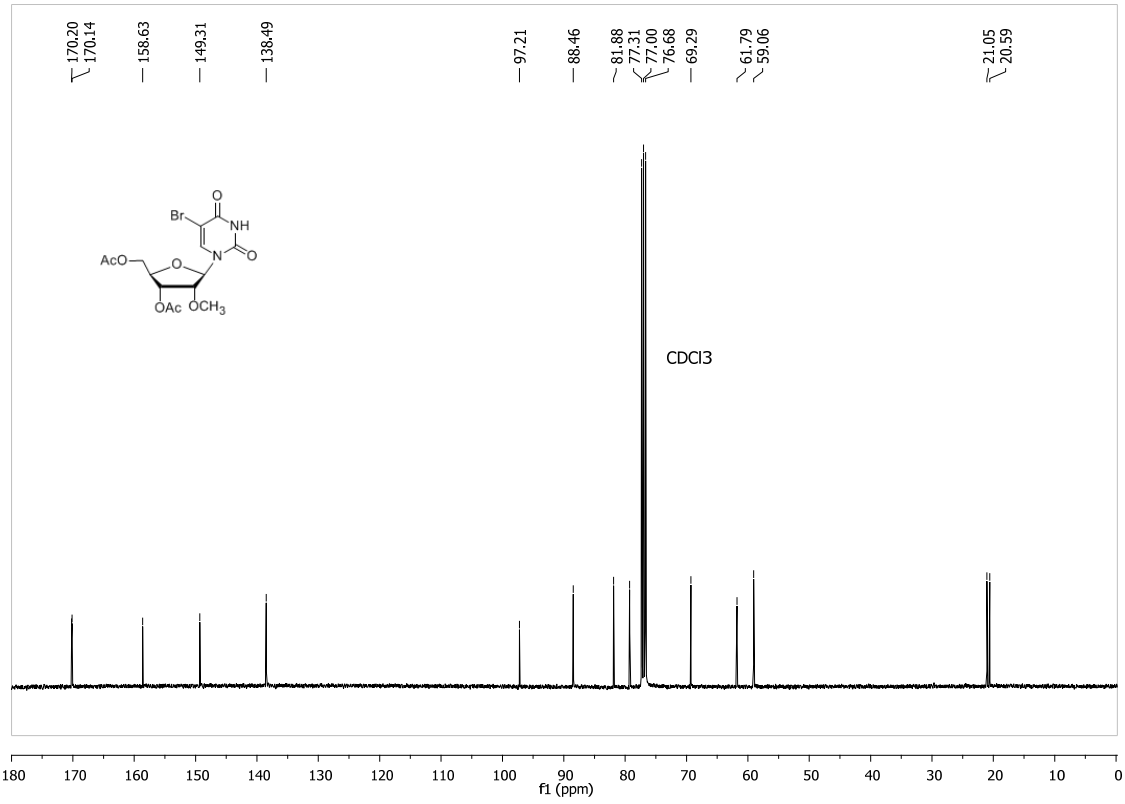

Figure S15. ^{13}C NMR spectrum of **3**

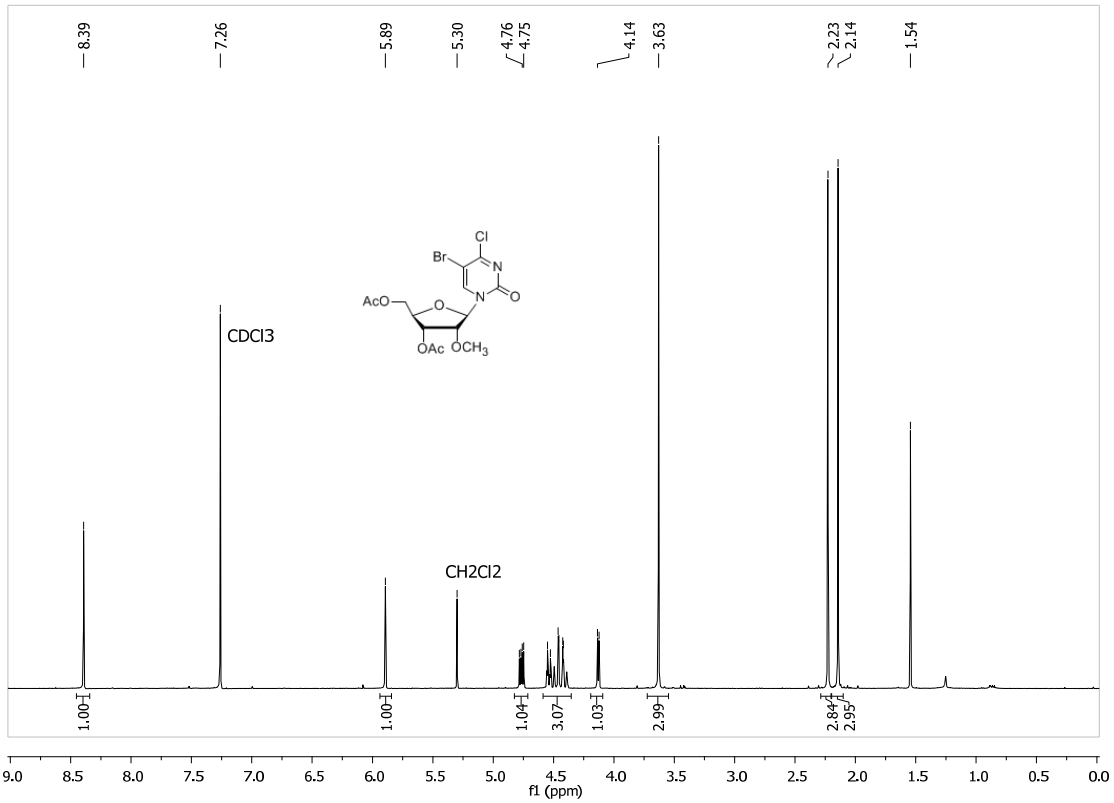

Figure S16. ^{1}H NMR spectrum of **4**

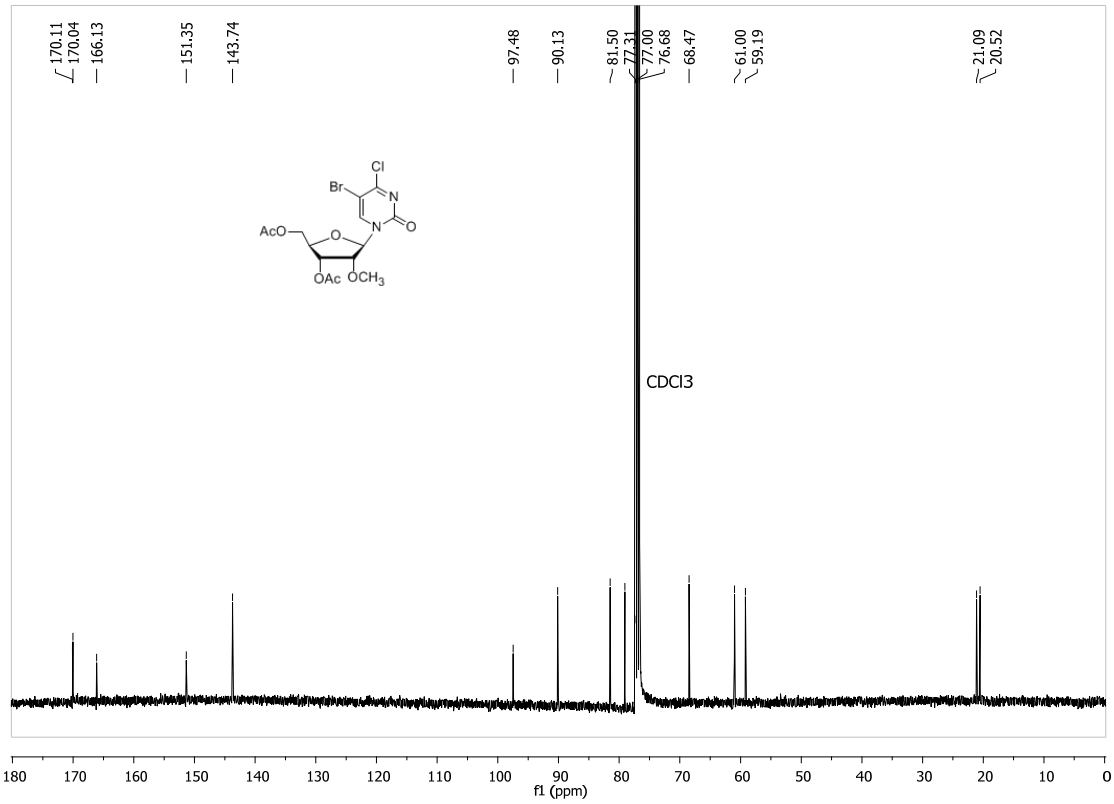

Figure S17. ^{13}C NMR spectrum of **4**

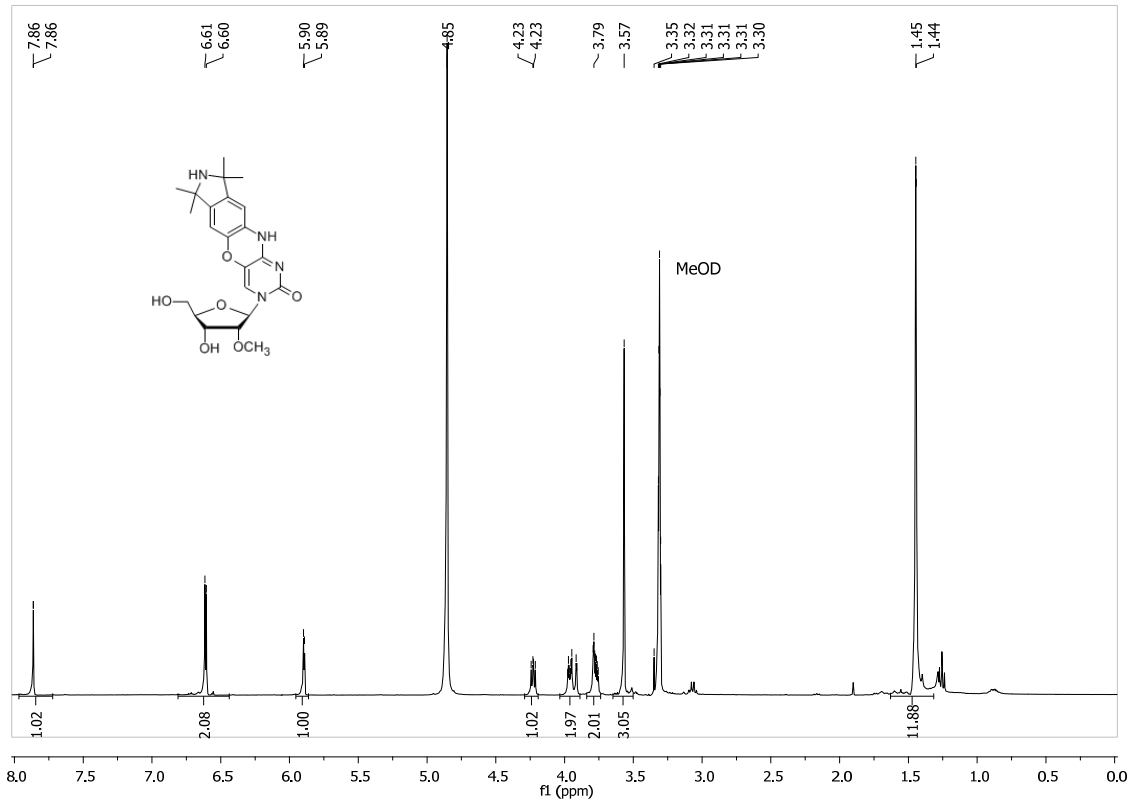

Figure S18. ^{1}H NMR spectrum of **7**

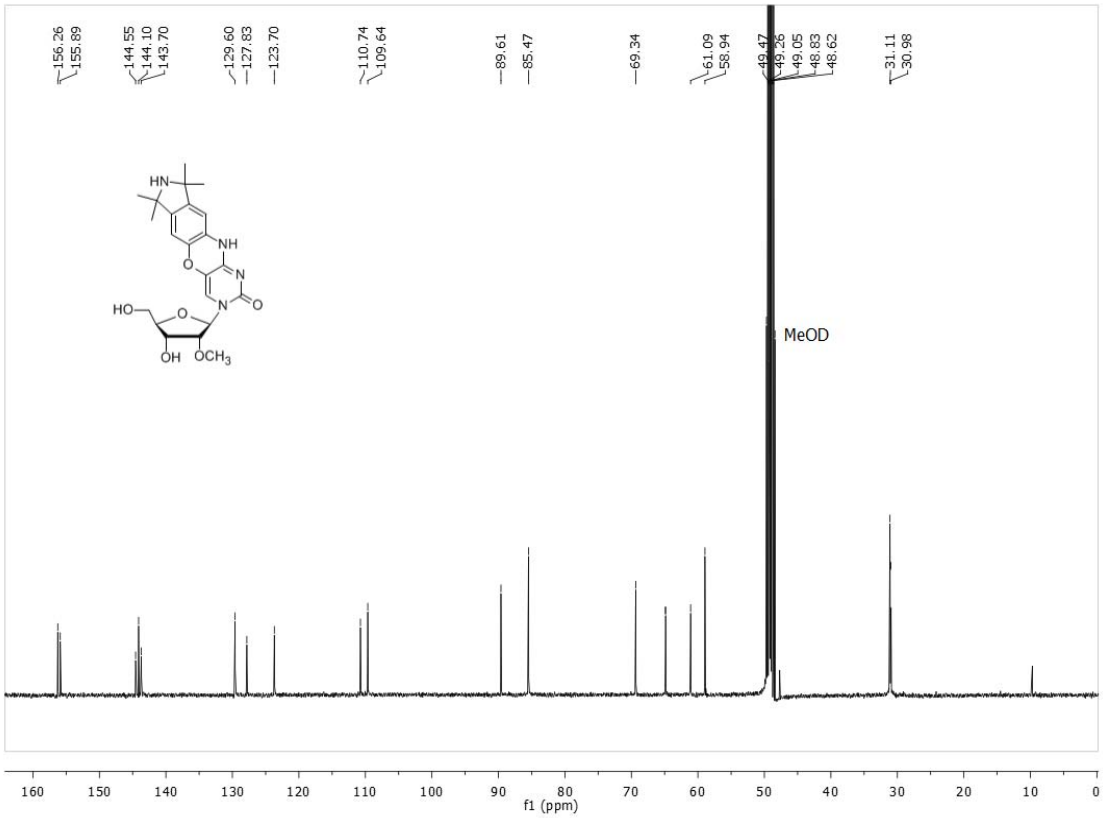

Figure S19. ^{13}C NMR spectrum of **7**

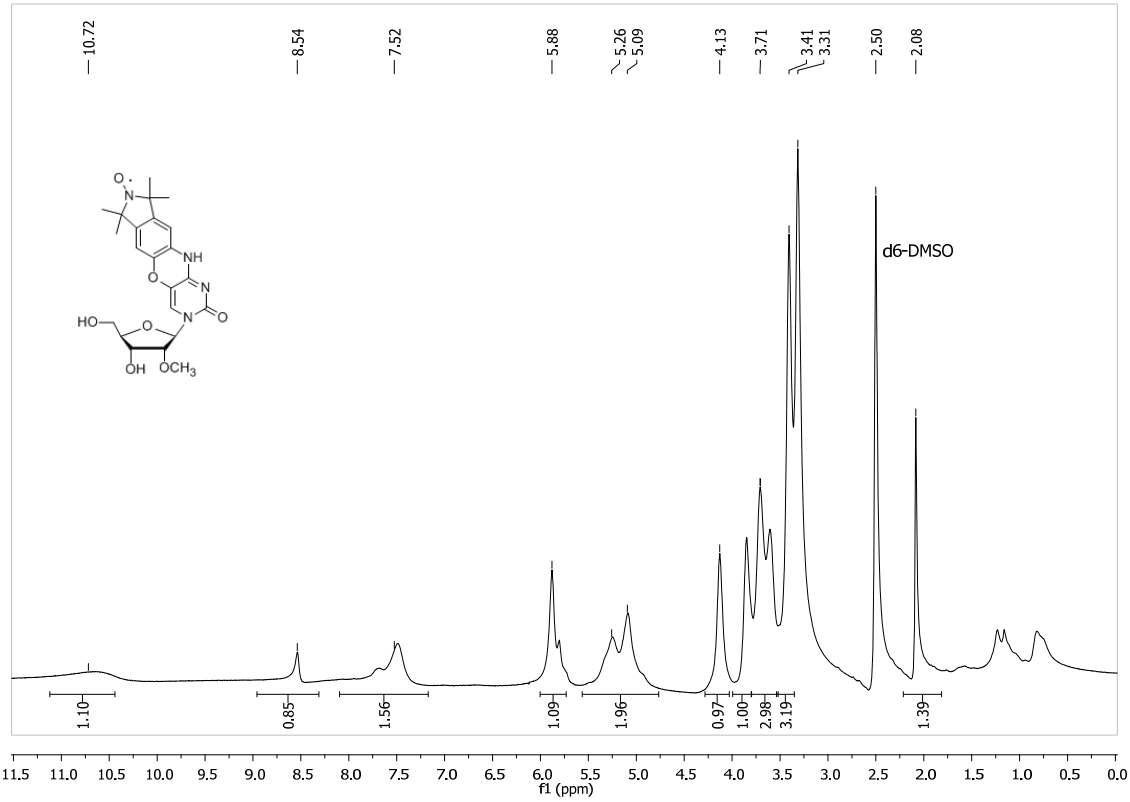

Figure S20. ^{1}H NMR spectrum of **Çm**

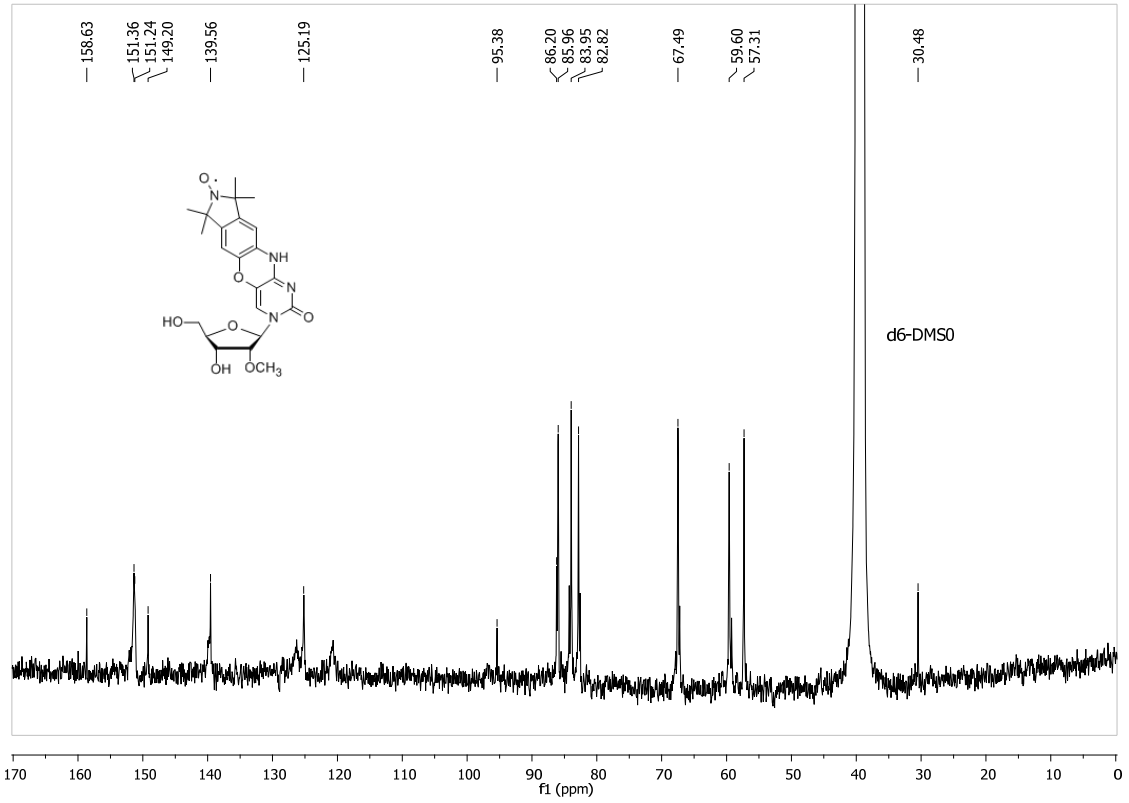

Figure S21. ^{13}C NMR spectrum of **Çm**

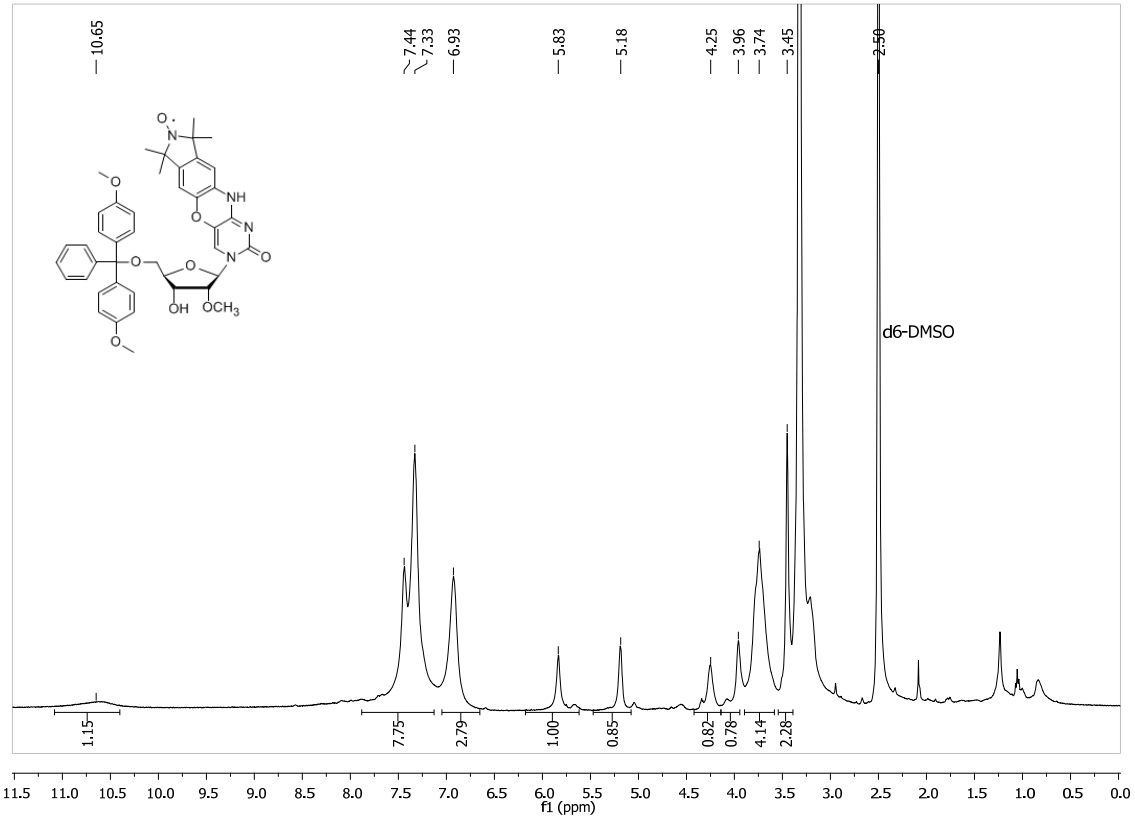

Figure S22. ^{1}H NMR spectrum of **tritylated Çm**

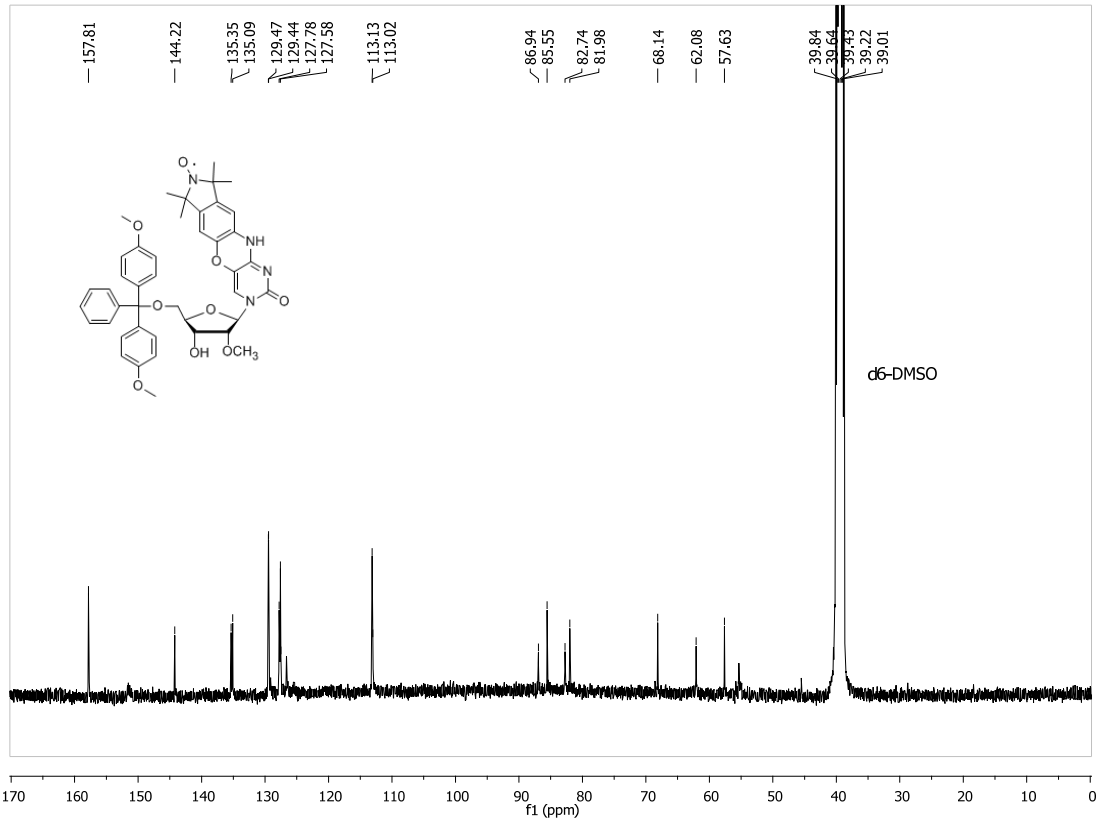

Figure S23. ^{13}C NMR spectrum of **tritylated Çm**

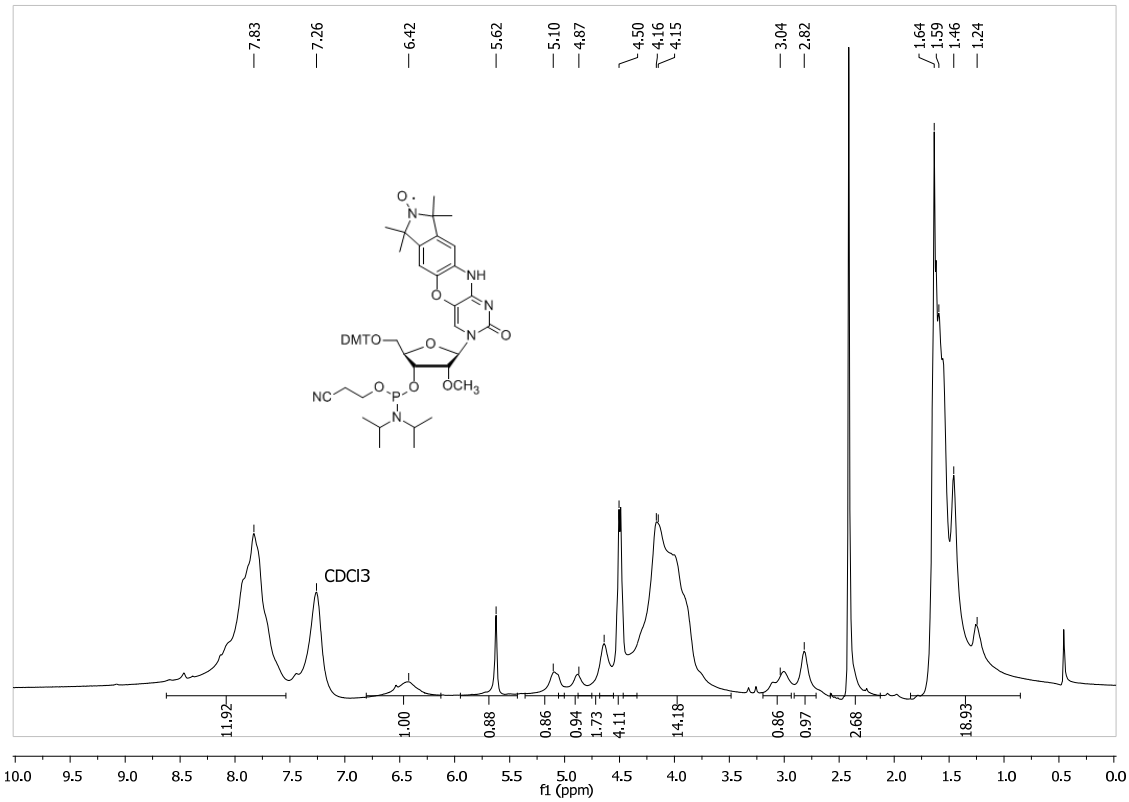

Figure S24. ^{1}H NMR spectrum of **Çm phosphoramidite 1**

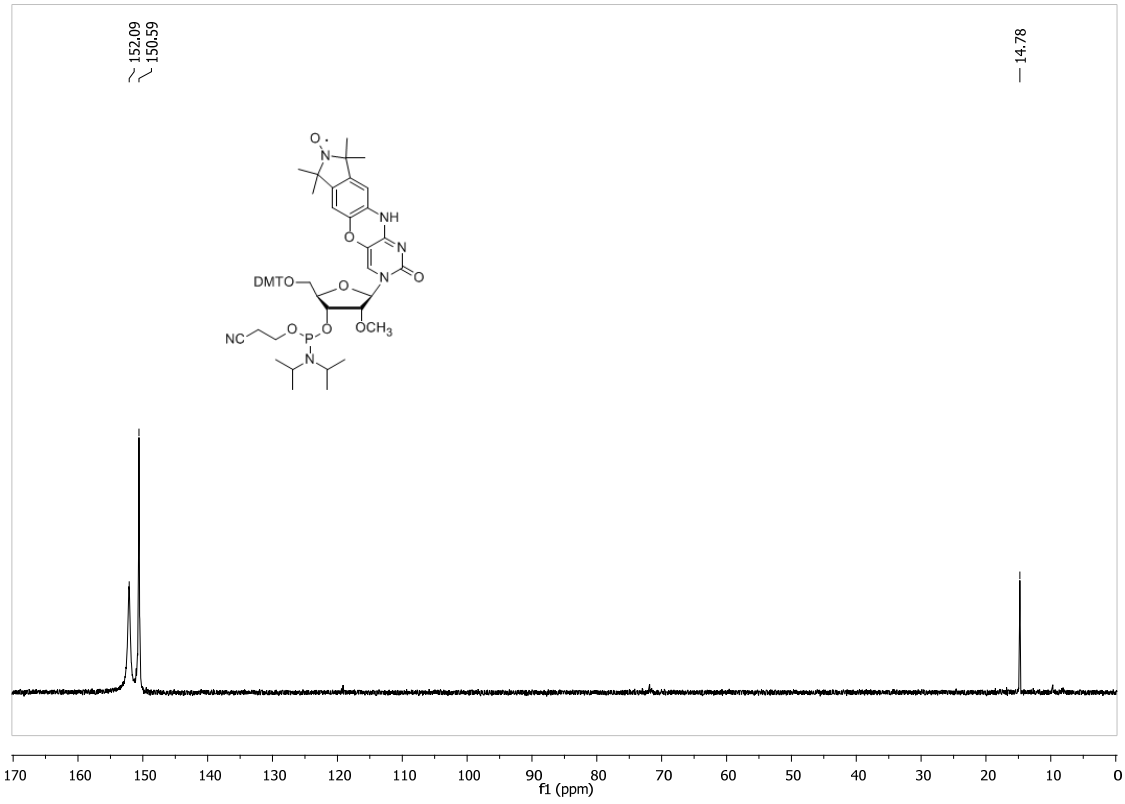

Figure S25. ^{31}P NMR spectrum of **Çm phosphoramidite 1**